EXPLORING MACHINE-LEARNING-ENABLED LIBS TOWARDS FORENSIC TRACE ATTRIBUTIVE ANALYSIS OF FISSION PRODUCTS IN SURROGATE HIGH-LEVEL NUCLEAR WASTE

Joshua Nyairo Onkangi*, Hudson Kalambuka Angeyo

Department of Physics, University of Nairobi, Nairobi Kenya;
e-mail: joshuanyairo@students.uonbi.ac.ke

We investigated the utility of machine-learning-enabled LIBS for direct rapid analysis of selected fission products (FPs), namely Y, Sr, Rb, and Zr in surrogate high-level nuclear waste mimicking three hypothetical but realistic scenarios: post-detonation glass debris, post-detonation powders, and microliter liquid drops from a radiological crime scene (RCS). Artificial neural network calibration strategies for trace quantitative analysis of the FPs in these materials were developed and achieved >95% prediction for all sample types. Owing to a lack of appropriate certified reference materials synthetic reference standards materials were used to perform method validation to accuracies >91%. Based on the spectral responses of the FPs, principal component analysis successfully differentiated nuclear from non-nuclear waste, demonstrating the method's potential for RCS nuclear forensic and attributive analysis.

Keywords: *laser-induced breakdown spectroscopy, artificial neural networks, principal component analysis, machine learning, nuclear forensics and attribution, high-level nuclear waste, fission products.*

ИСПОЛЬЗОВАНИЕ МАШИННОГО ОБУЧЕНИЯ НА БАЗЕ ЛАЗЕРНО-ИСКРОВОЙ ЭМИССИОННОЙ СПЕКТРОСКОПИИ ДЛЯ ПРОВЕДЕНИЯ СУДЕБНО-МЕДИЦИНСКОГО АТРИБУТИВНОГО АНАЛИЗА ПРОДУКТОВ ДЕЛЕНИЯ В СУРРОГАТНЫХ ВЫСОКОАКТИВНЫХ ЯДЕРНЫХ ОТХОДАХ

J. N. Onkangi*, H. K. Angeyo

УДК 543.423;621.039

Университет Найроби, Найроби, Кения; e-mail: joshuanyairo@students.uonbi.ac.ke

(Поступила 16 февраля 2022)

Исследована применимость лазерно-искровой эмиссионной спектроскопии и машинного обучения для прямого быстрого анализа отдельных продуктов деления (FP), а именно Y, Sr, Rb и Zr, в суррогатных высокоактивных ядерных отходах (постдетонационные обломки стекла, постдетонационные порошки и капли жидкости (в мкл) с места радиологического воздействия (RCS)). Разработаны стратегии калибровки искусственной нейронной сети для количественного анализа следов FP в этих материалах, которые позволили достичь прогнозирования >95 % для образцов всех типов. Из-за отсутствия соответствующих сертифицированных стандартных образцов для валидации метода использованы синтетические стандартные образцы с точностью ~91 %. На основании спектральных характеристик FP с помощью анализа главных компонент дифференцированы ядерные и неядерные отходы, продемонстрирован потенциал метода для ядерной судебной экспертизы и атрибутивного анализа RCS.

Ключевые слова: *лазерно-искровая эмиссионная спектроскопия, искусственные нейронные сети, анализ главных компонент, машинное обучение, ядерная криминалистика и атрибуция, высокоактивные ядерные отходы, продукты деления.*

Introduction. The current global nuclear renaissance has led to the growing use and trans-border movement of nuclear and radioactive materials (NRMs) for their various applications, resulting in the increased possibility of the illicit use of such materials [1, 2]. NRMs may be diverted from storage facilities or enrichment stages while in transit to repository sites, or during reprocessing of spent reactor fuel. In particular, the special nuclear materials (SNMs) uranium and plutonium need to be highly secured to enhance a safe nuclear regime. Nonetheless, should such materials be involved in a nuclear security event and are intercepted, there is a need for a method for direct and rapid nuclear forensic analysis and attribution. Most current nuclear forensic (NF) analytical techniques such as inductively coupled plasma-mass spectrometry (ICP-MS) provide accurate results but they require complex sample pre-treatments; thus, the integrity of the samples is compromised. Also, they lack the remote capability needed for NRMs. The remote ability of laser-induced breakdown spectroscopy (LIBS) makes it suitable for measurements at high temperatures or in environments with high radioactivity (e.g., inside a reactor) [3]). As NRM particles are representative of the original material, their analytical attributes can provide specific information about their sources in which regard attribution of post-detonation debris is desirable; measuring bulk samples runs the risk of averaging contributions of different (fallout) sources.

Laser-induced breakdown spectroscopy possesses remarkable attributes in this regard. It is versatile and can directly and simultaneously perform elemental, isotopic, and molecular analysis of solid and liquid samples in real-time, non-invasive mode [4]. The theory of LIBS has been extensively described [5, 6]. However, appropriate methods are needed to realize in particular portable LIBS for single-shot in-field applications of interest to nuclear forensics. Despite its advantageous attributes, however, LIBS has only rarely been investigated for nuclear forensic glass analysis [7–10]. LIBS has also been used for in situ analysis of radioactive surrogates on building bricks, pavements, and traffic signs [11], including those embedded in glass [9].

A typical RCS is characterized by samples of limited size (particulate matter, liquid droplets, and debris), which may yield only subtle LIBS analyte peaks buried in the pronounced background. Accurate trace quantification of fission products using LIBS in such cases is a challenge. Machine-learning methods are handy in facilitating the extraction of information from such spectra, including performing multivariate calibration [12]. In LIBS, thousands of data are collected in typically a second, constituting a complex spectrum [13]; it is, therefore, a natural extension to use machine-learning methods for dimensionality reduction as well as to aid interpretation [14].

Laser-induced breakdown spectroscopy has been applied in the analysis of uranium in glass matrices with an emphasis on investigating spectral interference [7]. The study of fission products (FPs) in ‘trinitite’ glass has been reported by Molgaard et al. and Hanson [15, 16]. Machine-learning techniques were used to associate spent fuel and the reactor type of origin based on the FP Inventory Code (FISPIN) [12]. Instead of using simulation codes, it is feasible to perform nuclear forensics utilizing real samples prepared to mimic those expected in the actual nuclear crime scenarios. This study focuses on cross-analyzing FPs in nuclear glass, powders, and liquid aliquots that have relevance in nuclear forensics. Fused glass offers a more physically stable matrix that gives more reliable spectral responses than sample forms such as pellets [17]. Artificial neural network (ANN) modeling was used to develop calibration strategies for trace quantitative analysis of the FPs in surrogate high-level nuclear waste in the absence of clearly observable LIBS peaks (peak-free LIBS). The attractions of ANN in multivariate calibration [18, 19] include the ability of neural networks to rapidly learn from input–output relationships as well as to model nonlinear data [20]. Principal component analysis (PCA) was used for data visualization in a graphical interface in a reduced dimension to more clearly discern any patterns that have the potential for nuclear forensic signature attribution. Three hypothetical but realistic nuclear security scenarios were mimicked: post-detonation scenes involving nuclear devices such as radiological dispersal devices (RDDs), re-detonation scenes in which a suspected NRM is intercepted, and accidental or intentional spillage of liquid NRM. As such cases are characterized by limited samples (tiny glass debris, powder particles, liquid droplets) for analysis and attribution of the NRM, a suitable NF methodology is desirable.

Materials and methods. Calibration samples were prepared using analytical grade standards namely RbCl, $SrCl_2 \cdot 6H_2O$, ZrO (Aldrich, USA), $Y(NO_3)_2 \cdot 5H_2O$ (Sigma-Aldrich, Germany), UO_3, $UO_2(NO_2) \cdot 6H_2O$ (BDH, England). Randomized concentrations were generated in Microsoft Excel covering the range 10–1000 ppm, which are typical for the Sr, Rb, and Y in reprocessed high-level nuclear waste (HLNW). Zr concentration was higher (up to 4000 ppm) as it is the main cladding for nuclear fuel pellets [21]. The simulated FPs were spiked on a 0–5% augmented natural uranium (grade) matrix, formulated to mimic HLNW arising from the reprocessing of a pressurized heavy water reactor (PHWR) with a burn-up of

7000 MW d/t U, a concentration of 250 L HLLW/t U, and a cooling period of 20 years [22]. The PHWR directly utilizes uranium in its natural form as fuel; therefore, the composition of the fuel is similar to that of yellow cake. The resultant mixture was placed in a mixer with a drill machine rotating for 5 min to homogenize. Each sample was prepared in three replicates. The first set was mixed with lithium metaborate (fluxing agent) and other glass-forming matrices SiO_2, $CaCO_3$, $NaCO_3$, and Al_2O_3. A micropipette was used to add 200 µL of potassium bromide as a nonwetting agent to facilitate the separation of glass from the crucible after fusion. The mixture was put into a Pt-Au crucible (2.5 mL capacity) and introduced into a pre-heated Nabertherm furnace at 1050°C and fused for 180 s. The alumina plate containing the samples was then withdrawn slowly to minimize recrystallization and sample fracturing and allowed to cool to room temperature. The procedure was repeated for the remaining samples. Thirty (30) fused glass (∅ 3 mm) samples (mimicking the borosilicate glass used to contain FPs) were prepared.

The second set was thoroughly mixed with cellulose powder and using 10 tons of hydraulic pressure, the mixture was pressed into pellets (~0.3 g) of 1.0 cm in diameter. Cellulose powder was used additionally to mimic one of the concealed forms in which NRM may be smuggled: the material may be mixed with powders, trafficked as that or as tablets and subsequently recovered through extraction at the destination. The cellulose-to-sample ratio was maintained at 5:1.

The third set of samples simulated high-level liquid nuclear waste (HLLNW). 0.1 g of the sample containing the FPs (Sr, Rb, Zr, Y) and uranium (U) was treated with 3M nitric acid to mimic the HLLNW slurry type that results from the reprocessing of spent fuel [23]. The diluent (nitric acid) to sample ratio was 5:1. Through a micropipette, small liquid aliquots (2 µL) were carefully deposited on the Perspex wafer to form a drop coat deposit (DCD) for subsequent LIBS analysis.

Sample analysis was realized using an appropriately optimized Q-switched and pulsed Nd:YAG laser (Ocean Optics Inc.) operating at a fundamental wavelength of 1064 nm. The pulse repetition frequency was 10 Hz, the laser pulse energy was 42.5 mJ, the Q switch delay was 150 µs, and the integration time was 0.42 s. The emitted radiation was collected by means of an optic fiber (with fused silica with a 0.22 numerical aperture and a focal length of 101 mm) positioned perpendicular to the direction of microplasma evolution. The spectrometer has a broad-band 7-CCD coupled system spanning the wavelength range 200–980 nm at ~0.065 nm resolution. This wavelength range contains most of the analytically useful lines required for LIBS analysis of most materials in the air at atmospheric pressure. The spectrometers acquire data through the OOILIBS software to help to identify the emitted photons, and compare and match with an existing database of atomic and molecular emissions.

Multivariate analyses of LIBS spectra. Machine-learning analysis of the LIBS spectra utilized spectral feature selection of regions of interest enveloping the analyte peaks (both the discernible and subtle) corresponding to Y, Sr, Rb, and Zr. The spectra were pre-processed using normalization and baseline restoration procedures. A representative region of the spectrum acquired by LIBS from a simulated HLLNW drop-coated on Perspex is shown in Fig. 1. Some FP interference-free peaks are discernible and are shown.

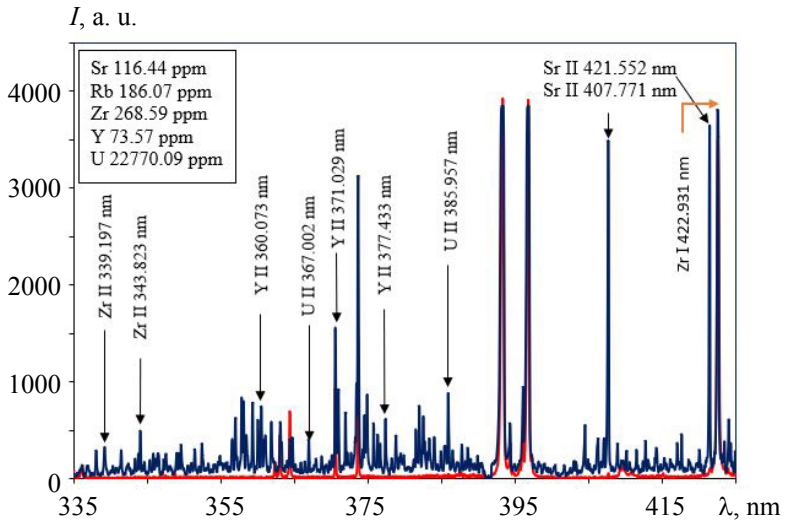

Fig 1. Example of FP spectral lines excited from simulated HLLW drop-coated on Perspex.

Artificial neural networks are nonlinear computational tools with the capability of modeling complex phenomena and hence are suitable for processing noisy and fuzzy data by emulating human cognitive processes. In addition, ANNs are valuable in nonlinear ordination, data visualization, and the development of hybridized deductive models [14].

Artificial neural networks consist of a huge number of parallel-connected arithmetic units called neurons with the capability of building an empirical multivariate calibration model of the form [24]:

$$\mathbf{Y} = f(\mathbf{X}) + \varepsilon, \quad (1)$$

where **Y** is the matrix of the response variables (known concentrations), *f* refers to the network function, and **X** is the input matrix (LIBS selected spectral features for input into MATLAB 7.8.0 (R2009a in our case); ε is the calibration error. Spectral feature selection not only highlights the analyte signatures to be modeled but also reduces data redundancy to achieve a more robust model. Feed-forward backpropagation algorithm and cascade correlation algorithms were compared for robustness. Although the backpropagation algorithm converges more easily [17, 18] the feed-forward one was found to be better. Two layers were used. The known concentrations of the analytes were treated as network targets. Three neurons were used, with a learning rate of 0.001. Sixty percent of the data was used for training, 25% for model testing; the remaining 15% was used for model validation. Models that gave the minimum square error were utilized for prediction. For the lack of an appropriate certified reference material (CRM), synthetic SRMs of the ICP and atomic absorption spectroscopy (AAS) solutions containing the FPs were used for model validation. The predictive ability of the developed ANN models was examined using three figures of merit: the limit of detection (LOD) calculated according to the criteria published in Choi et al. [7], the coefficient of determination (R^2), and the relative error of prediction (REP) [25].

As the combination of PCA is widely applied in spectroscopy before prediction by the use of multivariate techniques [26], this method was used for dimensionality reduction; mathematically, it realizes orthogonal transformation, which creates new uncorrelated variables to successively maximize the variance in the analyzed data. The principal components (PCs) describe the information hidden in a system of characteristic but partly dependent variables (each component is a weighted linear combination of the original variables). PCA, therefore, offers an avenue via which multivariate data can be explored to discover latent patterns as it is an unsupervised method.

The HLLNW samples with known concentrations of the FPs were used together with the reference blank matrix composed of pure 3M nitric acid as model inputs. Instead of feature selection as in the ANN modeling, the spectrum region containing most of the analyte spectral lines (300–400 nm) was selected for 14 samples (9 spiked with FPs, 5 blanks) and used in the PCA modeling in R studio Version 1.0.143 with the ‘Chemospec’ package [16]. Three samples were randomly selected from the dataset to be used for model validation. Figure 2 summarizes the framework for the analysis of the FPs using machine-learning-enabled LIBS.

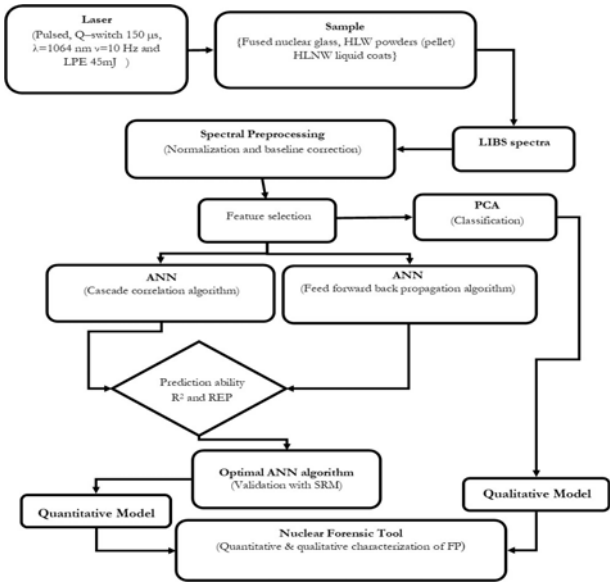

Fig. 2. Conceptual workflow for the detection and quantification of FPs in surrogate high-level nuclear waste utilizing machine-learning-enabled LIBS.

Results and discussion. Those LIBS FP lines that showed analytically useful spectral responses are shown in Fig. 3. The purpose of studying the spectral responses of these lines as a function of analyte (FP) concentration was to identify, based on the highest spiked concentrations, the regions of interest to guide the use of spectral feature selection in building the ANN models for the analysis of samples where such peaks are subtle and/or not discernible owing to the pronounced background and unexpected matrix spectral interference. LIBS spectra of such matrices are complex and require tailor-made calibration models based on the diversity of matrix-matched sample suites [27].

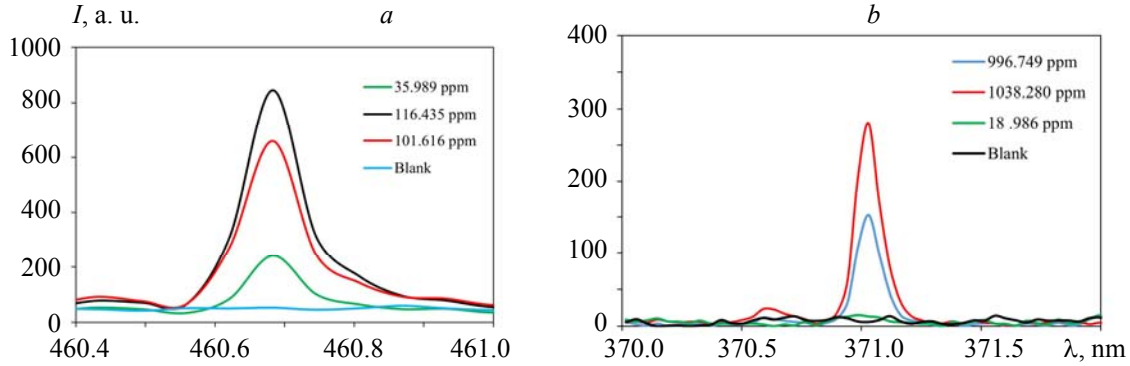

Fig 3. Selected (a) Sr spectral line λ = 460.733 nm and (b) Y spectral line λ = 371.029 nm showing the spectral response variations with respect to the concentration in fused glass.

Univariate calibration strategies [28, 29] and the calibration-free LIBS technique [30, 31] are characterized by inaccuracies and high detection limits when subtle analyte peaks are involved. LIBS also suffers from shot-to-shot irreproducibility, which further complicates the desired linear relationships between intensity and analyte concentration. Because LIBS spectra are multi-dimensional, they are amenable to a pipeline utilizing multivariate chemometrics [32–34]. In this work, ANN multivariate calibration models were used to circumnavigate these challenges.

Multivariate calibration for trace quantitative analysis using ANN. The performance of the developed ANN models for each of the FPs is summarized in Table 1. The R^2 values were > 0.95 for most of the models, illustrating the robustness of ANN compared with univariate calibration, which, as discussed above, is not feasible in this case. Selected examples of ANN regression performance curves are shown in Fig. 4. REP values for new sets of samples introduced into the model are given in Table 2. The values for drop deposits on Perspex were lowest compared with fused glass and pellets, which is attributed to reduced matrix effects. LIBS of glass is accompanied by fluorescence and quenching, which interfere with the analyte lines [35]. Fusing glass, however, does not eliminate matrix effects, it only reduces inconsistencies in the absorption of the laser energy and minimizes the saturation of strong and resonance peaks [17].

TABLE 1. Model Performance Based on the Explained Variance (R^2), Relative Error of Prediction (REP) and Limit of Detection LOD for Fused Glass, Pellet and Drop-Coatings on Perspex.

Element	Fused glass			Pelletized form			Drop-coat on Perspex		
	R^2	REP, %	LOD, ppm	R^2	REP, %	LOD, ppm	R^2	REP, %	LOD, ppm
Sr	0.939	12.350	175.0	0.974	8.730	18.8	0.957	1.470	6.5
Rb	0.985	9.610	181.0	0.991	5.560	25.5	0.897	11.680	6.0
Y	0.984	3.780	129.1	0.999	31.060	70.1	0.977	12.350	7.2
Zr	0.987	7.300	199.1	0.750	15.020	67.7	0.957	4.180	54.6

TABLE 2. HLLW Model Validation Using Synthetic SRM

Standard solution	Certified standard concentration, ppm	Average predicted (Triplicate), ppm	Deviation from the certified value, %
Sr-ICP standard	100	91.34±2.34	8.66
Z-AAS standard	500	542.14±5.51	8.43
Y-ICP standard	100	93.61±4.14	6.39

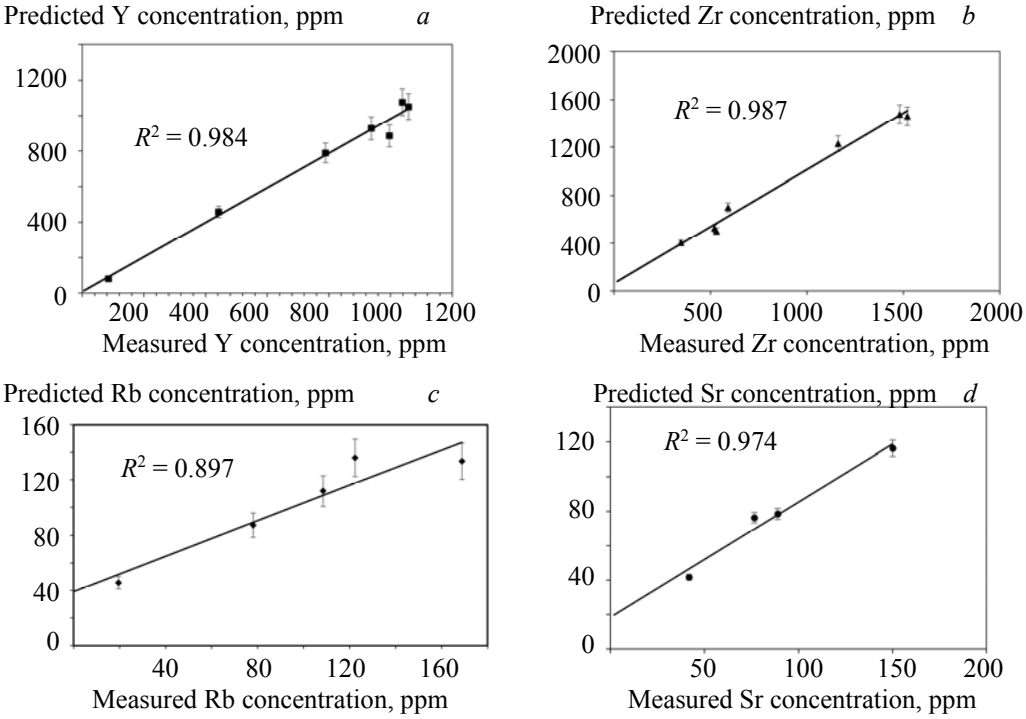

Fig 4. Selected ANN regression performance curves for (a) Y and (b) Zr in fused nuclear glass samples, (c) Rb in drop liquid aliquot deposited on Perspex, and (d) Sr in a pellet sample (simulated nuclear powder) utilizing LIBS spectral feature selection.

The prediction power of the ANN model in real samples was done for the DCDs using a synthetic ICP standard solution (CertiPUR® MERCK) developed via a methodology similar to that used for the simulated liquid samples. This was done because, just like for the glass and pellet samples analyzed in this work, a CRM for high-level liquid nuclear waste was not available. The concentrations of Sr, Y, and Zr had <9% deviation from the SRM values (Table 2). REP values for dry micro-drop deposits on Perspex agreed closely with the results obtained using the synthetic SRM solutions.

PCA of surrogate HLNW samples. In a typical nuclear security scenario, for example, a detonated nuclear device/radiological crime scene, the contents of the material involved get jumbled and it is hard to separately sample each for laboratory analysis. If data from such samples is acquired, then pattern recognition can be explored to reveal trends (e.g., the relationship between samples collected, the FP present). PCA can be used to help to visualize such relationships. Figure 5a shows the scores plot for 9 samples spiked with FPs and 5 blanks. It was noted that 75% of the variation in the data is captured by the first and second PCs. The rest of the variation (25%) is associated with other PCs, noise, and matrix-related influences. The liquid samples spiked with trace quantities (<1000 ppm) of the FP cluster together (SL group). The blank samples also cluster together (BL group). The loadings plot shows that the peaks of Y and Zr, together with U, account for the positive PC-1 clustering, as shown in Fig. 5b.

The PCA model was further tested using new samples (SLT1 and SLT3). These grouped together with the spiked liquid samples whereas the blank sample (LBT2) clustered with the blank liquid samples. This observation is important in nuclear forensic analysis because it demonstrates that samples that are suspected to originate from a nuclear security scene can be identified and discriminated against those that do not contain FPs. Notably, spectra of tiny liquid aliquots (2 μL) collected from a radiological scene can be sampled and deposited on a suitable substrate and compared with the reference spectral database to furnish a nuclear forensic interpretation that leads to attribution. It has been shown [36] that it is possible to simulate post-blast residues of non-nuclear origin with the use of PCA, underscoring the utility of machine-learning-enabled nuclear forensic analysis.

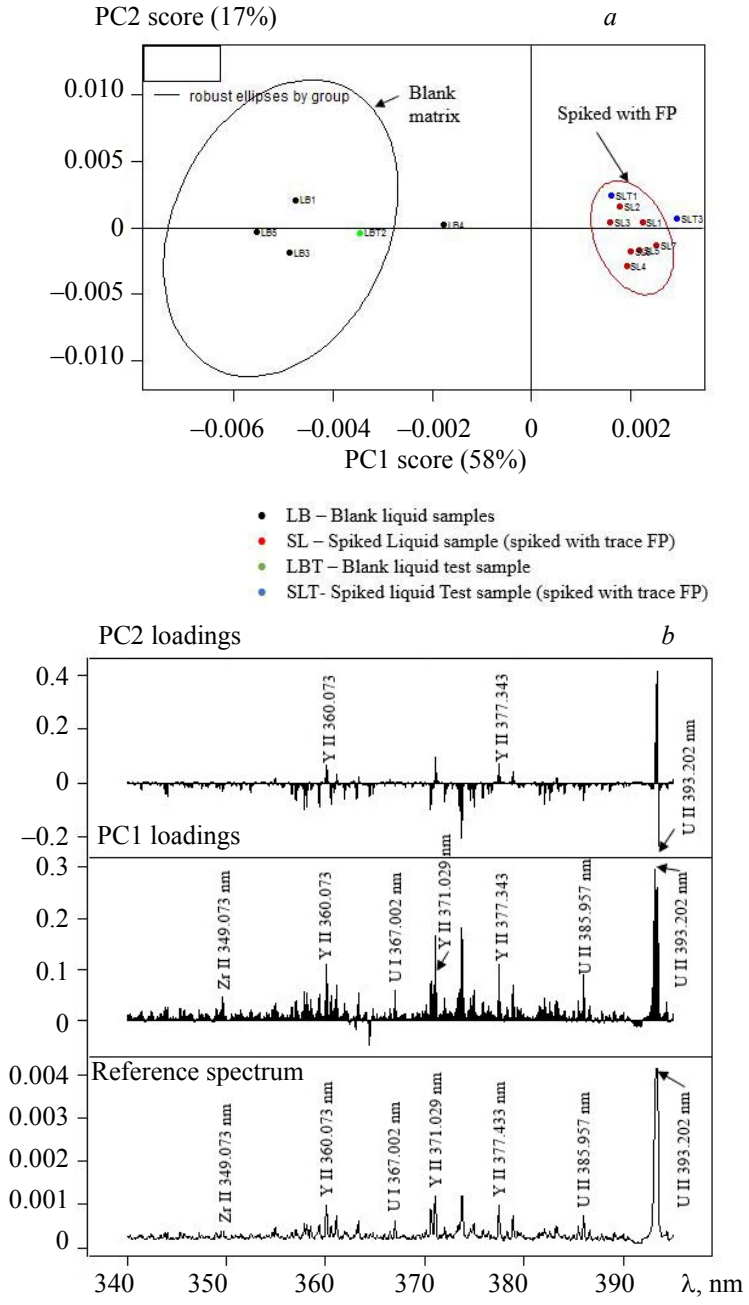

Fig 5. (a) PCA scores plot to simulate high-level liquid nuclear waste and (b) the corresponding loadings plot for PC1 and PC2 for simulated high-level nuclear liquid waste.

Conclusions. We have demonstrated proof-of-concept for a machine-learning-enabled laser-induced breakdown spectroscopy methodology for directly analyzing and attributing fission products (Rb, Sr, Y, Zr) in surrogate high-level nuclear waste. These fission products always coexist with U following reprocessing of the high-level nuclear waste. The proposed analytical framework is rapid as there is limited sample preparation. The novelty of the methodology lies in the reliance on tiny samples (∅3 mm for solid samples, and typically 2 μL for liquid samples) to achieve direct, non-invasive, and potentially in situ nuclear forensics analysis and attribution. Artificial neural networks were found to be useful in developing accurate regression models that predict and quantify trace fission products in the samples. Principal component analysis was used to discriminate the samples containing trace FPs from those without them based on the spectral feature selection criterion. The spectral peaks from Y, Zr, and U are responsible for the observed grouping and

therefore they depict powerful nuclear forensics signatures for high-level nuclear waste. The results demonstrate the potential of machine-learning-enabled peak-free laser-induced breakdown spectroscopy for the forensic analysis of nuclear debris.

Acknowledgments. The authors wish to acknowledge The World Academy of Sciences for Advancement of Science in Developing Countries (TWAS) and the Kenya Nuclear Electricity Board (KNEB) for financing the research work in the form of an MSc fellowship to the first author. Equally, the authors acknowledge the Laser Physics and Spectroscopy Group of the Department of Physics, University of Nairobi, and the Institute of Nuclear Science & Technology, University of Nairobi fraternity, including the late David Maina, for providing equipment that enabled the completion of this research.

REFERENCES

1. H. K. Angeyo, *Int. J. Nucl. Secur.*, **4**, No. 1, Article 2 (2018).
2. M. Miller, *Nonproliferation Rev.*, **14**, No. 1, 33–60 (2007), doi: 10.1080/10736700601178465.
3. Y.-S. Kim et al., *Spectrochim. Acta B: At. Spectrosc.*, **74**, 90–193 (2012).
4. S. Rai, A. K. Rai, *AIP Adv.*, **1**, No. 4, 042103 (2011).
5. D. A. Cremers, L. J. Radziemski, *Handbook of Laser-Induced Breakdown Spectroscopy*, John Wiley & Sons (2013).
6. R. E. Russo, X. L. Mao, H. C. Liu, J. H. Yoo, S. S. Mao, *Appl. Phys. A*, **69**, No. 1, S887–S894 (1999).
7. I. Choi, G. C.-Y. Chan, X. Mao, D. L. Perry, R. E. Russo, *Appl. Spectrosc.*, **67**, No. 11, 1275–1284 (2013), doi: 10.1366/13-07066.
8. P. Devangad et al., *Opt. Mater.*, **52**, 32–37 (2016).
9. E. C. Jung, D. H. Lee, J.-I. Yun, J. G. Kim, J. W. Yeon, K. Song, *Spectrochim. Acta B: At. Spectrosc.*, **66**, No. 9, 761–764 (2011).
10. X. Wang et al., *Spectrochim. Acta B: At. Spectrosc.*, **87**, 139–146 (2013).
11. I. Gaona, J. Serrano, J. Moros, J. J. Laserna, *Spectrochim. Acta B: At. Spectrosc.*, **96**, 12–20 (2014).
12. A. E. Jones, P. Turner, C. Zimmerman, J. Y. Goulermas, *Anal. Chem.*, **86**, No. 11, 5399–5405 (2014).
13. N. Labbé, I. M. Swamidoss, N. André, M. Z. Martin, T. M. Young, T. G. Rials, *Appl. Opt.*, **47**, No. 31, G158–G165 (2008).
14. H. K. Angeyo, International Atomic Energy Agency (IAEA) International Conference on Nuclear Security: Enhancing Global Efforts, Vienna, Austria, 1–5 July (2013).
15. J. J. Molgaard et al., *J. Radioanal. Nucl. Chem.*, **304**, No. 3, 1293–1301 (2015).
16. B. A. Hanson, *Package Version*, 2 (2014).
17. P. Pease, *Spectrochim. Acta B: At. Spectrosc.*, **83**, 37–49 (2013).
18. M. Cilimkovic, *Inst. Technol. Blanchardstown Blanchardstown Road North Dublin*, **15**, No. 1 (2015) [Online]. Available: https://drive.uqu.edu.sa/_/takawady/files/NeuralNetworks.pdf
19. V. Skorpil, J. Stastny, "Back-Propagation and K-Means Algorithms Comparison," presented at the 8th Int. Conf. Signal Processing (2006).
20. R. N. Naguib, G. V. Sherbet, *Artificial Neural Networks in Cancer Diagnosis, Prognosis, and Patient Management*, CRC Press (2001).
21. A. M. Bevilacqua, N. B. M. de Bernasconi, M. E. Sterba, "Desarrollo de la Formulación y Preparación de Residuos Simulados de Alta Actividad Tipo PHWR," Bariloche, Argentina (1987).
22. M. J. Bell, "ORIGEN: the ORNL isotope generation and depletion code," Oak Ridge National Lab. (1973).
23. M. A. Audero, A. M. Bevilacqua, N. B. de Bernasconi, D. O. Russo, M. E. Sterba, *J. Nucl. Mater.*, **223**, No. 2, 151–156 (1995).
24. F. Marini, R. Bucci, A. L. Magrì, A. D. Magrì, *Microchem. J.*, **88**, No. 2, 178–185 (2008).
25. N. C. Dingari, G. L. Horowitz, J. W. Kang, R. R. Dasari, I. Barman, *PLoS One*, **7**, No. 2, e32406 (2012).
26. S. D. Kamath, C. S. D'souza, S. Mathew, S. D. George, C. Santhosh, K. K. Mahato, *J. Chemom. J. Chemom. Soc.*, **22**, No. 6, 408–416 (2008).
27. B. Sallé, J.-L. Lacour, P. Mauchien, P. Fichet, S. Maurice, G. Manhes, *Spectrochim. Acta B: At. Spectrosc.*, **61**, No. 3, 301–313 (2006).
28. D. A. Cremers, F.-Y. Yueh, J. P. Singh, H. Zhang, *Laser-Induced Breakdown Spectroscopy, Elemental Analysis*. Wiley Online Library, 2006. Accessed: Jul. 19 (2015). [Online]. Available: http://onlinelibrary.wiley.com/doi/10.1002/9780470027318.a0708.pub2/full

29. A. Haider, M. Wahadoszamen, M. E. Sadat, K. M. Abedin, A. I. Talukder, *Opt. Laser Technol.*, **42**, No. 6, 969–974 (2010).
30. A. Ciucci, M. Corsi, V. Palleschi, S. Rastelli, A. Salvetti, E. Tognoni, *Appl. Spectrosc.*, **53**, No. 8, 960–964 (1999).
31. P. Yaroshchyk, D. Body, R. J. Morrison, B. L. Chadwick, *Spectrochim. Acta B: At. Spectrosc.*, **61**, No. 2, 200–209 (2006).
32. S. M. Clegg, E. Sklute, M. D. Dyar, J. E. Barefield, R. C. Wiens, *Spectrochim. Acta B: At. Spectrosc.*, **64**, No. 1, 79–88 (2009).
33. M. Z. Martin, N. Labbé, T. G. Rials, S. D. Wullschleger, *Spectrochim. Acta B: At. Spectrosc.*, **60**, No. 7-8, 1179–1185 (2005).
34. J.-B. Sirven, B. Salle, P. Mauchien, J.-L. Lacour, S. Maurice, G. Manhes, *J. Anal. At. Spectrom.*, **22**, No. 12, 1471–1480 (2007).
35. D. Alamelu, A. Sarkar, S. K. Aggarwal, *Talanta*, **77**, No. 1, 256–261 (2008).
36. K. Banas et al., *Anal. Chem.*, **82**, No. 7, 3038–3044 (2010).